Vehicle-To-Everything Downlink and Uplink Communication Using Multi-Carrier Rate-Splitting

Derek Kwaku Pobi Asiedu, Yun Ji-Hoon, Benjillali Mustapha, Samir Saoudi

Vehicle-To-Everything Downlink and Uplink Communication Using Multi-Carrier Rate-Splitting

Derek Kwaku Pobi Asiedu*, Ji-Hoon Yun†, Mustapha Benjillali‡*, and Samir Saoudi*
*IMT-Atlantique, Lab-STICC, 29238 Brest, France. Emails: kwakupobi@ieee.org, and samir.saoudi@imt-atlantique.fr
†Department of Electrical and Information Engineering, SeoulTech, Seoul 01835, South Korea. Email: jhyun@seoultech.ac.kr
‡ Department of Communication Systems, INPT, Rabat 10100, Morocco. Email: benjillali@ieee.org

***Abstract*—To highlight the potential of RSMA and multi-carrier (MC) techniques in vehicle-to-everything (V2X) communication, we propose and present a two-way communication MC-RSMA V2X communication system that supports a large number of equipments (UEs) and promotes the dual function of sidelink and cellular communication. We employ k-mean clustering for vehicle grouping and a suboptimal sub-carrier allocation with naive equal time and optimal precoder design for data transfer. To confirm the efficacy of the proposed system model, we compare the MC-RSMA solution against an MC-SDMA benchmark, using sum-rate as the performance metric. From the simulation results, the proposed system demonstrates significant improvements over the two multi-access technique benchmarks.**

***Index Terms*—Vehicle-to-everything, sum-rate, rate-splitting multiple access, orthogonal frequency division multiple access.**

I. Introduction

The advancement of vehicle-to-everything (V2X) communication has brought significant benefits to road safety, climate sustainability, and intelligent transportation systems [1], [2]. V2X communication encompasses vehicle-to-vehicle (V2V), vehicle-to-network (V2N), vehicle-to-infrastructure (V2I), vehicle-to-roadside unit (V2R), and vehicle-to-pedestrian (V2P) communications [2]–[4]. In V2X communication, cellular communication involves user equipment (UEs) (e.gs., smart devices, road side unit, and vehicles) communicating through the BS, while sidelink (i.e., device-to-device (D2D)) communication involves V2V communication [2]–[4].

Two radio access technologies are commonly used in V2X deployments. The first is the Dedicated Short Range Communication (DSRC) standard, which supports D2D communication [1]–[3], [5]. The second standard supports cellular communication (i.e., C-V2X). Currently, fifth-generation (5G) new radio (NR) C-V2X standards are being proposed to support services such as vehicle platooning, remote driving, and direct communication interface enhancement [1]–[3], [5]. The next evolution is the proposal of sixth-generation C-V2X standards, which will involve improved C-V2X communication quality-of-service (QoS) and efficiency resource usage, support a numerous UE simultaneous communication using multi-access techniques such as rate splitting multiple access (RSMA), which can jointly support cellular and sidelink communication.

RSMA is an appealing technology for V2X communication due to key advantages, such as; RSMA enables multi-casting [6], [7], RSMA is robust against mobility imperfections [6], and RSMA promotes efficient spectrum and network resource utilization [8], [9]. This highlights the potential opportunities for further research on RSMA in V2X communication applications and standardizations. Now, by combining RSMA with multi-carrier (MC) techniques such as orthogonal frequency division multiple access (OFDMA) will further increase these benefits. The scalability of MC-RSMA allows for better joint cellular and sidelink communication, user grouping, and resource management, which are essential features for future 6G V2X communication technologies and standards. Therefore, utilizing MC-RSMA in V2X communication is imperative.

II. Related Works

Research on RSMA in V2X includes works in [6]–[10]. In [6], the focus was on designing DL RSMA communication between a massive multiple-input-multiple-out (mMIMO) transmitter and mobile UEs, using both previous and current time-slot channel state information (CSI) to account for imperfections due to user mobility. In [7], the authors maximized the weighted joint sum-rate and sum-MSE (minimum squared error) for a joint cellular and radar system based on power allocation and successful common stream decoding. The work in [10] extended [7] to a generalized case with imperfect CSI (imp-CSI). In [8], the authors discussed an RSMA-specified satellite-to-ground (UEs and moving target) waveform optimization and focused on the Dual-functional radar-communication (DFRC) beamforming optimization by minimizing the Cramer-Rao bound, with per-UE rate constraints. Additionally, [9] investigated an energy-efficient generalized DFRC with low-resolution digital-to-analogue converter and radio frequency (RF) chain selection. RSMA implementation can be done using either a single-carrier (SC) approach [6], [7] or a multi-carrier (MC) approach [11], [12]. Research on MC-RSMA has mainly focused on multi-user (MU)-MISO general cellular communication, with [11] optimizing power and sub-carrier allocation for sum-rate maximization and [12] optimizing power allocation to maximize capacity.

From the above discussion, this paper is the first to delve into the joint MC-RSMA DL and uplink (UL) with sidelink V2X communication system model, opening up a vast realm of possibilities for future V2X studies and standards. This paper proposes a novel approach to V2X diverse-casting communi-

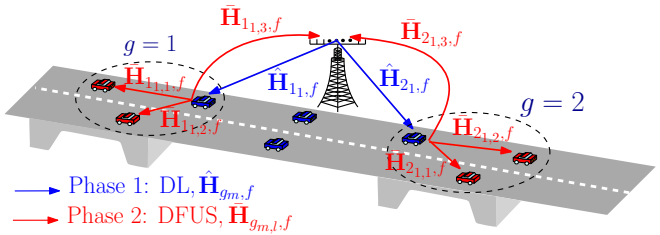

Fig. 1. The two-way MC-RSMA MV2X communication illustration.

cation using MC-RSMA transmitter architecture, MU-MIMO (multiple V2X (MV2X) communications), user grouping, and resource allocation (i.e., power and sub-carrier). This work covers, an mMIMO base station (BS) performing first phase DL communication with several groups of vehicles using MC-RSMA. The second phase involves the DL vehicles using MC-RSMA to simultaneously perform BS UL and perform sidelink communication with other vehicles, which has not been considered in previous works.

Notations: l_2-norm is denoted by $\|.\|$. Capital and lowercase bold letters (Greek and Roman) represent matrices and vectors, respectively. Scalar variables are represented by normal letters. The trace and determinant of matrix $\mathbf{A}$ are denoted as $\text{tr}(\mathbf{A})$ and $\det(\mathbf{A})$, respectively. The Hermitian of $\mathbf{A}$ is denoted as $\mathbf{A}^H$, and $\mathbf{A} \in \mathbb{C}^{M\times N}$ denotes an $M \times N$ complex matrix. $\mathcal{CN}(\mu, \sigma^2)$ represents a Circularly Symmetric Complex Gaussian (CSCG) distribution with mean μ and variance σ^2.

III. Proposed MC-RSMA V2X Communication

A. The Two-Way MC-RSMA MV2X Architecture

The two-way MC-RSMA MV2X system model considered is illustrated in Fig. 1. The two-way time division duplexing communication consists of MC-RSMA DL (phase one) and MC-RSMA dual function of combined UL and sidelink (DFUS) (phase two) communication. Specifically, phase one DL communication occurs between the BS and grouped MV2X. While the second phase DFUS occurs between the grouped MV2X performing UL and sidelink communication with BS and other vehicles, respectively.

Phase one communication consists of an N_{BS} antenna BS and K UEs (vehicles) with $N_{\text{BV},k}$ antennas, where $N_{\text{BS}} \geq \sum_{k=1}^{K} N_{\text{BS},k}$. Note, the UEs are clustered into G groups and allocated $\mathcal{S}_g$ sub-carriers per group g ($g = 1, \ldots, G$) out of F sub-carriers. Each group g has M_g UEs, with the mth UE labelled UE_{g_m} ($m = 1, \ldots, M_g$), and the RSMA DL common and private channel for UE_{g_m} over sub-carrier $f \in \mathcal{S}_g$, ($f = 1, \ldots, F$) are defined as $\hat{\mathbf{H}}_{g_m,f} = [\hat{\mathbf{H}}_{g^c_m,f}, \hat{\mathbf{H}}_{g^p_m,f}]$, where c and p represent the common and private messages of the RSMA technique, respectively. During phase two DFUS communication, each UE_{g_m} uses its allocated $\mathcal{S}_g$ to transmit signals to its L_{g_m} DFUS receivers (i.e., $\text{UE}_{g_{m,l}}$, $l = 1, \ldots, L_{g_m}$, consisting of vehicles with $N_{\text{V},l}$ antennas and the BS). The common and private channels for phase two are defined as $\bar{\mathbf{H}}_{g_{m,l},f} = [\bar{\mathbf{H}}_{g^c_{m,l},f}, \bar{\mathbf{H}}_{g^p_{m,l},f}]$. Next, the details of the two-way communication is presented. The MC-RSMA transmission and reception architectures are shown in Fig. 2 and the 1-layer RSMA architecture is adopted in the system model.

B. Phase 1: DL Communication

Step 1, DL UE grouping and sub-carrier allocation: The UE grouping is based on K-mean clustering using the first sub-carrier channel characteristic (i.e., $\hat{\mathbf{H}}_{k^p,1}, \forall k$) out of the F sub-carriers. Meaning, a sub-carrier will be shared by either a group or all of UEs ($G \leq K$ and $\sum_{g=1}^{G} M_g = K$). After the UE grouping, the sub-carriers are allocated based on G.

Step 2, group g MC-RSMA, $\forall g$: The messages intended for UE_{g_m} is defined as $Q_{g_m} = \min(N_{BS}, \min\{N_{BV,k}\}_{\in g})$. Note, the size of all messages of group g must be $Q_{g^p} = \min(N_{BS}, \sum_{m=1}^{M_g} Q_{g_m})$. First, UE_{g_m} messages, $\mathbf{w}_{g_m} = \{w_1, \ldots, w_{Q_{g_m}}\}$, are split into the common ($\mathbf{w}_{g^c_m}$) and private ($\mathbf{w}_{g^p_m}$) messages. Next, all group g common messages are combined into $Q_{g^c} \in \{1, \ldots, \min(N_{BS}, \min\{N_{BV,k}\}_{\in g})\}$ messages denoted as $\mathbf{w}_{g^c}$. The $\{\mathbf{w}_{g^p_m}\}_{m=1}^{M_g}$ and $\mathbf{w}_{g^c}$ messages are then encoded as $\mathbf{s}_{g^c} \in \mathbb{C}^{Q_{g^c}\times 1}$ and $\mathbf{s}_{g^p_m} \in \mathbb{C}^{Q_{g_m}\times 1}$, respectively. Therefore, the resulting data stream to be transmitted is expressed as $\mathbf{s}_g = [\mathbf{s}_{g^c}, \mathbf{s}_{g^p_1}, \ldots, \mathbf{s}_{g^p_M}]^T$.

Step 3, group g OFDM, $\forall g$: The encoded data streams are passed to the Orthogonal frequency division multiplexing (OFDM) system before transmission [13]. Group g data stream, $\mathbf{s}_g$, is precoded, such that, $\mathbf{x}_{g,f} = \hat{\mathbf{P}}_{g,f}\mathbf{s}_g$, where $\hat{\mathbf{P}}_{g,f} = [\hat{\mathbf{P}}_{g^c,f}, \hat{\mathbf{P}}_{g^p_1,f}, \ldots, \hat{\mathbf{P}}_{g^p_M,f}]$ is the precoder matrix for group g on the sub-carrier f, $\mathbb{E}[\mathbf{s}_g\mathbf{s}_g^H] = \mathbf{I}$ and $\mathbb{E}[\mathbf{P}_{g,f}\mathbf{P}_{g,f}^H] = P_{T,f}$. $\mathbf{P}_{g^c,f} \in \mathbb{C}^{N_{BS}\times Q_{g^c}}$ and $\mathbf{P}_{g_m,f} \in \mathbb{C}^{N_{BS}\times Q_{g_m}}$ are the common and private messages precoders for group g, respectively. $P_{T,f}$ is the power allocated to sub-carrier f. Afterwards, the Inverse Fast Fourier Transform (IFFT) conversion operation occurs on the precoded parallel data allocated to sub-carrier f. The converted data stream has the cyclic prefix (CP) appended and transmitted from the BS to all UEs in group g. The process is repeated at the BS for all G groups.

Step 4, UE_{g_m} OFDM: First the CP is removed from the received data at UE_{g_m}, then Fast Fourier Transform (FFT) conversion is performed [13] on group g received data on their allocated sub-carriers ($\mathcal{S}_g \subseteq \{1, \ldots, F\}$). Hence, the received data stream at UE_{g_m} over sub-carrier $f \in \mathcal{S}_g$ is given as

$$\mathbf{y}_{g_m,f} = \hat{\mathbf{H}}_{g_m,f}\mathbf{x}_{g,f} + \mathbf{n}_{g_m,f}, \tag{1}$$

where $\mathbf{n}_{g_m,f} \sim \mathcal{CN}(0, \sigma^2_{g_m})$ is the Additive White Gaussian Noise (AWGN) at UE_{g_m} over sub-carrier f.

Step 5, UE_{g_m} RSMA decoding: The received data, $\mathbf{y}_{g_m,f}$ is then decoded as follows. The common message is decoded as $\hat{\mathbf{w}}_{g^c,f}$ by treating all the private messages as interference. The common messages are removed from the received data stream $\mathbf{y}_{g_m,f}$ using successive interference cancellation (SIC). UE_{g_m} then extracts its common message, $\hat{\mathbf{w}}_{g^c_m,f}$, from $\hat{\mathbf{w}}_{g^c,f}$. Next, the private messages of UE_{g_m} is decoded as $\hat{\mathbf{w}}_{g^p_m,f}$ by treating the private messages of other UEs $\in g, \forall f \in \mathcal{S}_g$ as noise. Note that this process is repeated for all sub-carriers allocated to group g, where $\text{UE}_{g_m} \in g$. Finally, all decoded $\hat{\mathbf{w}}_{g^c_m,f}$ and $\hat{\mathbf{w}}_{g^p_m,f}$ for $\mathcal{S}_g$ sub-carriers are combined to estimate massage $\hat{\mathbf{w}}_{g_m}$ intended for UE_{g_m}. This process is repeated at all G groups and UEs to decode their intended messages.

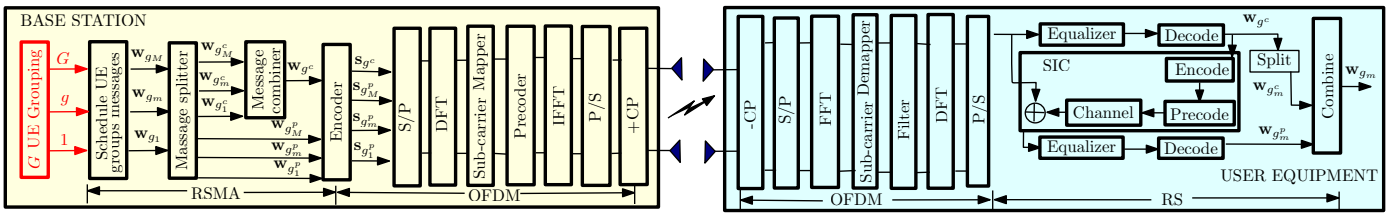

Fig. 2. Proposed MC-RSMA communication architecture.

Sum-rate formulation: Using the minimum mean square error (MMSE) receiver at UE$_{g_m}$ [14], the estimated common and private messages after SIC and decoding are

$$\begin{aligned}\hat{\mathbf{s}}_{g_m^c,f} &= \mathbf{V}_{g_m^c,f}\mathbf{y}_{g_m,f} \text{ and}\\ \hat{\mathbf{s}}_{g_m^p,f} &= \mathbf{V}_{g_m^p,f}(\mathbf{y}_{g_m,f} - \hat{\mathbf{H}}_{g_m,f}\hat{\mathbf{P}}_{g^c,f}\mathbf{s}_{g_m^c,f}),\end{aligned} \tag{2}$$

with common and private messages receive filters $\mathbf{V}_{g_m^c,f} \in \mathbb{C}^{Q_{g^c}\times Q_{g_m}}$ and $\mathbf{V}_{g_m^p,f} \in \mathbb{C}^{Q_{g^p}\times Q_{g_m}}$, respectively. The MSE of UE$_{g_m}$ for both the common and private streams is given as

$$\xi_{g_m^z,f} = \mathbb{E}[\|\hat{\mathbf{s}}_{g_m^z,f} - \mathbf{s}_{g_m^z,f}\|^2],\ f \in \mathcal{S}_g,\ z \in \{c,p\}. \tag{3}$$

By differentiating the MSEs with respect to (w.r.t) their receiver filter, the optimal receiver filters are deduced as

$$\mathbf{V}_{z_1,f}^{\text{opt}} = \hat{\mathbf{P}}_{z_2,f}^H\hat{\mathbf{H}}_{g_m,f}^H(\hat{\mathbf{H}}_{g_m,f}\hat{\mathbf{P}}_{z_2,f}\hat{\mathbf{P}}_{z_2,f}^H\hat{\mathbf{H}}_{g_m,f}^H + \mathbf{\Lambda}_{z_1,f})^{-1}, \tag{4}$$

where $(z_1,z_2) \in \{(g_m^c,g^c),(g_m^p,g_m^p)\}$,
$\mathbf{\Lambda}_{g_m^c,f} = \mathbf{I} + \sum_{i=1}^{M_g}\hat{\mathbf{H}}_{g_m,f}\hat{\mathbf{P}}_{g_i^p,f}\hat{\mathbf{P}}_{g_i^p,f}^H\hat{\mathbf{H}}_{g_m,f}^H$, and
$\mathbf{\Lambda}_{g_m^p,f} = \mathbf{I} + \sum_{i\neq m}^{M_g}\hat{\mathbf{H}}_{g_m,f}\hat{\mathbf{P}}_{g_i^p,f}\hat{\mathbf{P}}_{g_i^p,f}^H\hat{\mathbf{H}}_{g_m,f}^H$. Now, substituting $\mathbf{V}_{z_1,f}^{\text{opt}}$ into the MSE equations results in

$$\mathbf{\Theta}_{z_1,f} = (\mathbf{I} + \hat{\mathbf{P}}_{z_2,f}^H\hat{\mathbf{H}}_{g_m,f}^H(\mathbf{\Lambda}_{z_1,f})^{-1}\hat{\mathbf{H}}_{g_m,f}\hat{\mathbf{P}}_{z_2,f}). \tag{5}$$

Based on the MSE, the UE$_{g_m}$ common and private achievable rate for all allocated sub-carriers is given as

$$R_{z_1} \triangleq \sum_{f\in\mathcal{S}_g}\log\det[\mathbf{\Theta}_{z_1}]^{-1}. \tag{6}$$

The common rate shared by the UEs in group g is defined as $\sum_{m=1}^{M_g}\sum_{f\in\mathcal{S}_g}C_{g_m^c,f} = R_{g^c}$, where $C_{g_m^c,f}$ is the common rate of UE$_{g_m}$ over sub-carrier $f \in \mathcal{S}_g$. $R_{g^c} = \min_m\{\{\log\det(\mathbf{\Theta}_{z_1,f})^{-1}\}_{f\in\mathcal{S}_g}\}_{m=1}^{M_g}, \forall f \in \mathcal{S}_g$ is a constraint imposed on decoding the common message transmitted over all UE$_{g_m}$ allocated sub-carriers successful. UE$_{g_m}$ achievable rate is deduced as $R_{g_m} = \sum_{f\in\mathcal{S}_g}C_{g_m^c,f} + R_{g_m^p,f}$ and the total DL achievable rate is derived as

$$R_{\text{MC-RS}}^{\text{DL}} = \sum_{g=1}^{G}\sum_{m=1}^{M_g}\frac{\tau}{S_g}\sum_{f\in\mathcal{S}_g}C_{g_m^c,f} + R_{g_m^p,f}, \tag{7}$$

where, τ is the time allocated for phase 1 communication.

C. Phase 2: DFUS Communication

For the phase two DFUS communication, UE$_{g_m}$ transmits data simultaneously to the BS and other UEs (UE$_{g_{m,l}}$, $l \in L_{g_m}$) for UL and sidelink communication by using the $\mathcal{S}_g$ sub-carriers allocated to UE$_{g_m}$ in phase 1. In addition, the DFUS communication uses the MC-RSMA architecture presented in Fig. 2, except the user grouping, which is not applied because the DFUS has lesser receivers compared to phase one (i.e., $L_{g_m}+1 << K$). The DFUS communication achievable system rate is derived following the steps given in Section III-B.

UE$_{g_{m,l}}$ received data over sub-carrier f is given as

$$\mathbf{y}_{g_{m,l},f} = \bar{\mathbf{H}}_{g_{m,l},f}\mathbf{x}_{g_m,f} + \sum_{j\neq m}^{M_g}\bar{\mathbf{H}}_{g_{j,l},f}\mathbf{x}_{g_j,f} + \mathbf{n}_{g_{m,l},f}, \tag{8}$$

where $\mathbf{n}_{g_{m,l},f}$ is the AWGN noise at UE$_{g_{m,l}}$. From (8), the other UEs (UE$_{g_j}, j \neq m$) in group g with UE$_{g_m}$ introduce interference at UE$_{g_{m,l}}$. Next, the achievable rate of UE$_{g_{m,l}}$ is derived as $R_{g_{m,l}} = \sum_{f\in\mathcal{S}_g}C_{g_{m,l}^c,f} + R_{g_{m,l}^p,f}$, where $R_{g_{m,l}^p,f} \triangleq \log\det[\mathbf{\Theta}_{g_{m,l}^p,f}]^{-1}$ is UE$_{g_{m,l}}$ private message rate, and $C_{g_{m,l}^c,f}$ is the common message of UE$_{g_{m,l}}$ over sub-carrier f, such that, $\sum_{l=1}^{L_{g_m}+1}\sum_{f\in\mathcal{S}_g}C_{g_{m,l}^c,f} = R_{g_m^c}$, and $R_{g_{m,l}^c,f} = \min_l\{\{\log\det(\mathbf{\Theta}_{g_{m,l}^c,f})^{-1}\}_{f\in\mathcal{S}_g}\}_{l=1}^{L_{g_m}+1}, \forall f \in \mathcal{S}_g$. where $\mathbf{\Theta}_{z_1,f} = \mathbf{I} + \bar{\mathbf{P}}_{z_2,f}^H\bar{\mathbf{H}}_{g_{m,l},f}^H(\mathbf{\Lambda}_{z_1,f})^{-1}\bar{\mathbf{H}}_{g_{m,l},f}\bar{\mathbf{P}}_{z_2,f}$, $(z_1,z_2) \in \{(g_{m,l}^p,g_{m,l}^p),(g_{m,l}^c,g_m^c)\}$ with $\mathbf{\Lambda}_{z_1,f}$ defined in (9) and (10). The total DFUS achievable rate is given as

$$R_{\text{MC-RS}}^{\text{DFUS}} = \sum_{g=1}^{G}\sum_{m=1}^{M_g}\sum_{l=1}^{L_{g_m}}\frac{(1-\tau)}{S_g}\sum_{f\in\mathcal{S}_g}C_{g_{m,l},f} + R_{g_{m,l},f}. \tag{11}$$

D. Optimization Problem Definition

From (7) and (11), the two-way MC-RMSA MV2X system sum-rate (SR) optimization problem is given in (12), where χ consists of G, $\{\mathcal{S}_g\}_{g=1}^{G}$, $\hat{\mathbf{P}}_{g^c}$, $\{\bar{\mathbf{P}}_{g_m^c,f}\}_{g=1,m=1}^{G,M_g}$, $\{C_{g_m^c,f}\}_{g=1,m=1}^{G,M_g}$, $\{C_{g_{m,l}^c,f}\}_{g=1,m=1,l=1}^{G,M_g,L_{g_m}}$, $\{\hat{\mathbf{P}}_{g_m^p,f}\}_{g=1,m=1}^{G,M_g}$, and $\{\bar{\mathbf{P}}_{g_{m,l}^p,f}\}_{g=1,m=1,l=1}^{G,M_g,L_{g_m}}$. Constraints (12a) and (12b) are the DL and UE$_{g_m}$ DFUS power budgets respectively, which are convex functions. Constraint (12c), ensures that sub-carriers are allocated to UE groups based on total number of sub-carrier, F. Constraints (12d) and (12e) ensure that the common stream is successfully decoded for UE$_{g_m}$ and UE$_{g_{m,l}}$, respectively. Constraints (12f) and (12g) ensure that the decoded common messages rates for the DL and DFUS are not zero. Note that constraints (12c) to (12g) are monotonically increasing functions. The $\bar{R}_{\text{MC-RSMA}}^{\text{DL}}$ and $\bar{R}_{\text{MC-RSMA}}^{\text{DFUS}}$ are defined in (7) and (11), respectively, which are non-convex w.r.t. all dependent variables, meaning, Problem (12) is a non-convex.

IV. MC-RSMA V2X System Optimization

The proposed alternating optimization (AO) solution and algorithm to Problem (12) are summarized in this section.

$$\mathbf{\Lambda}_{g^p_{m,l},f} = \mathbf{I} + \sum_{i=1,i\neq l}^{L_{g_m}} \bar{\mathbf{H}}_{g_{m,l},f} \bar{\mathbf{P}}_{g^p_{m,i},f} \bar{\mathbf{P}}^H_{g^p_{m,i},f} \bar{\mathbf{H}}^H_{g_{m,l},f} + \sum_{j=1,j\neq m}^{M_g} \sum_{i=1}^{L_{g_j}} \left(\bar{\mathbf{H}}_{g_{j,i},f} \bar{\mathbf{P}}_{g^p_{j,i},f} \bar{\mathbf{P}}^H_{g^p_{j,i},f} \bar{\mathbf{H}}^H_{g_{j,i},f} + \bar{\mathbf{H}}_{g_{m,l},f} \bar{\mathbf{P}}_{g^c_j,f} \bar{\mathbf{P}}^H_{g^c_j,f} \bar{\mathbf{H}}^H_{g_{m,l},f} \right) \tag{9}$$

$$\mathbf{\Lambda}_{g^c_{m,l},f} = \mathbf{I} + \sum_{i=1}^{L_{g_m}} \bar{\mathbf{H}}_{g_{m,l},f} \bar{\mathbf{P}}_{g^p_{m,i},f} \bar{\mathbf{P}}^H_{g^p_{m,i},f} \bar{\mathbf{H}}^H_{g_{m,l},f} + \sum_{j=1}^{M_g} \sum_{i=1}^{L_{g_j}} \left(\bar{\mathbf{H}}_{g_{m,l},f} \bar{\mathbf{P}}_{g^p_{j,i},f} \bar{\mathbf{P}}^H_{g^p_{j,i},f} \bar{\mathbf{H}}^H_{g_{m,l},f} + \bar{\mathbf{H}}_{g_{m,l},f} \bar{\mathbf{P}}_{g^c_j,f} \bar{\mathbf{P}}^H_{g^c_j,f} \bar{\mathbf{H}}^H_{g_{m,l},f} \right) \tag{10}$$

$$\begin{aligned} &\underset{\chi}{\text{maximize}}\ \bar{R}^{\text{DL}}_{\text{MC-RS}} + \bar{R}^{\text{DFUS}}_{\text{MC-RS}} \text{ subject to } \sum_{g=1}^{G} \sum_{f=1}^{S_g} \Big[\sum_{m=1}^{M_g} \text{Tr}\Big(\hat{\mathbf{P}}_{g^p_m,f} \hat{\mathbf{P}}^H_{g^p_m,f} \Big) + \text{Tr}\Big(\hat{\mathbf{P}}_{g^c,f} \hat{\mathbf{P}}^H_{g^c,f} \Big) \Big] \leq P_T \ \text{(12a)}, \\ &\sum_{f=1}^{S_g} \Big[\sum_{l=1}^{L_{g_m,}} \text{Tr}\Big(\bar{\mathbf{P}}_{g^p_{m,l},f} \bar{\mathbf{P}}^H_{g^p_{m,l},f} \Big) + \text{Tr}\Big(\bar{\mathbf{P}}_{g^c_m,f} \bar{\mathbf{P}}^H_{g^c_m,f} \Big) \Big] \geq P_{T,g_m} \ \text{(12b)}, \ \sum_{g=1}^{G} S_g \leq F, \ 1 \leq S_g \leq F, \ \forall g, \ \text{(12c)}, \\ &\sum_{j=1,j\neq m}^{M_g} \sum_{f\in\mathcal{S}_g} C_{g^c_j,f} \leq R_{g^c}, \ \text{(12d)}, \ \sum_{i=1,i\neq l}^{L_{g_m}} \sum_{f\in\mathcal{S}_g} C_{g^c_{m,i},f} \leq R_{g^c_m}, \ \text{(12e)}, \ C_{g^c_m,f} \geq 0, \ \text{(12f)}, C_{g_{m,l},f} \geq 0, \ \text{(12g)}, \end{aligned} \tag{12}$$

A. DL UE Grouping and Sub-Carrier Allocation

1) User-grouping: The K-mean machine learning (ML) algorithm is used to determine the UE groups. Here the feature space is spanned by the normalized (complex-valued) first sub-carrier channel vector of the UE, $\hat{\mathbf{h}}_{k^p,1} = \text{vec}(\hat{\mathbf{H}}_{k^p,1})$. The set of normalized channel vectors denoted by $\aleph = \{\boldsymbol{\alpha}_k : \boldsymbol{\alpha}_k \triangleq \frac{\hat{\mathbf{h}}_{k^p,1}}{\|\hat{\mathbf{h}}_{k^p,1}\|} e^{-j\angle \hat{h}_{k^p,1}}, \forall k\}$ has each component phase-adjusted such that the first elements of all $\boldsymbol{\alpha}_k$'s aligned to 0 degrees. Note, the number of clusters $\mathcal{K}$ is predetermined, and is equal to the UE groups (i.e., $\mathcal{K} = G$).

2) Sub-carrier allocation: The sub-carrier allocation problem is defined as

$$\underset{\mathcal{S}_g}{\text{maximize}}\ \bar{R}^{\text{DL}}_{\text{MC-RS}} \ \text{ subject to (12c).} \tag{13}$$

Problem (13) is hard to solve, so, the suboptimal equal power sub-carrier allocation solution proposed in [15] is adopted using the UE with the highest sub-carrier channel gain ($\|\hat{\mathbf{H}}_{k^p,1}\|^2$) within a group as the allocation factor.

B. Sum-Rates Problem (SRP) Optimization

The sum-rate problem (SRP) is defined as

$$\begin{aligned} &\underset{\chi}{\text{maximize}}\ \bar{R}^{\text{DL}}_{\text{MC-RS}} + \bar{R}^{\text{DFUS}}_{\text{MC-RS}} \\ &\text{subject to} \quad \text{(12a), (12b), (12d), (12e), (12f), (12g),} \end{aligned} \tag{14}$$

with τ, g and S_g fixed. This implies that the $\bar{R}^{\text{DL}}_{\text{MC-RS}}$ and $\bar{R}^{\text{DFUS}}_{\text{MC-RS}}$ problems can be separated into Problems

$$\underset{\hat{\chi}}{\text{maximize}}\ \bar{R}^{\text{DL}}_{\text{MC-RS}} \text{ subject to (12a), (12d), (12f) and,} \tag{15}$$

$$\underset{\bar{\chi}}{\text{maximize}}\ \bar{R}^{\text{DFUS}}_{\text{MC-RS}} \text{ subject to (12b), (12e), (12g),} \tag{16}$$

and solved separately, where the dependent variables $\hat{\chi}$ consists of $\{C_{g^c_m,f}\}^{G,M_g}_{g=1,m=1}$, $\{\hat{\mathbf{P}}_{g^p_m,f}\}^{G,M_g}_{g=1,m=1}$, and $\{\hat{\mathbf{P}}_{g^c,f}\}^{G}_{g=1}$, and $\bar{\chi}$ includes $\{\bar{\mathbf{P}}_{g^c_m,f}\}^{G,M_g}_{g=1,m=1}$, $\{\bar{\mathbf{P}}_{g^p_{m,l},f}\}^{G,M_g,L_{g_m}}_{g=1,m=1,l=1}$, and $\{C_{g^c_{m,l},f}\}^{G,M_g,L_{g_m}}_{g=1,m=1,l=1}$. Both problems are non-convex, but are solved by converting both problems into convex weighted MMSE (WMMSE) problems. Both problems are similar in structure and solution derivation. Therefore, the solution of Problem (15) is presented for brevity and Problem (16) can be solved following the steps used in solving Problem (15).

Algorithm 1 MC-RSMA sum-rate maximization algorithm

1: Use set τ, $\{\hat{\mathbf{H}}_{k,f}\}^{K,F}_{k=1,f=1}$ and $\{\bar{\mathbf{H}}_{l,f}\}^{L,F}_{l=1,f=1}$
2: Given $\{\hat{\mathbf{H}}_{k^p,1}\}^{K}_{k=1}$ determine G using K-mean
3: Assign each sub-carrier f based on [15] algorithm, $\forall g$
4: Solve Problems (15) and (16) using WMMSE and CVX

Focusing on problem (15), the DL WMMSE is defined in (17), where $\delta_{g^c_m,f} = -C_{g^c_m,f}$, $\xi_{z_1,f} = \text{tr}(\mathbf{U}_{z_1,f}\Theta_{z_1,f}) - \log\det(\mathbf{U}_{z_1,f})$, $\mathbf{U}_{z_1,f}$ is the WMMSE weight and $z_1 \in \{g^p_m, g^c_m\}$. The optimal $\mathbf{U}_{z_1,f}$ and $\mathbf{V}_{z_1,f}$ are derived as

$$\begin{aligned} &\mathbf{U}_{z_1,f} = (\Theta_{z_1,f})^{-1}, \\ &\mathbf{V}_{z_1,f} = \hat{\mathbf{P}}^H_{z_2,f} \hat{\mathbf{H}}^H_{g_m,f} (\hat{\mathbf{H}}_{g_m,f} \hat{\mathbf{P}}_{z_2,f} \hat{\mathbf{P}}^H_{z_2,f} \hat{\mathbf{H}}^H_{g_m,f} + \mathbf{\Lambda}_{z_1,f})^{-1}, \end{aligned} \tag{18}$$

from Problem (17) Lagrangian and Karush–Kuhn–Tucker (KKT) conditions differential w.r.t. each variable, equated to zero and solving for the said variable.

Now, the power allocation and common rate problem is a convex Quadratically Constrained Quadratic Program (QCQP) defined in (19), and solved using CVX [14], with $(z_1, \hat{z}_1, z_2) = \{(g^p_m, f), (g^p_i, f), (g^c, f)\}$. The definition of the variables within the above equations are $\hat{\hat{\mathbf{p}}}_{z_1} = \text{vec}(\hat{\mathbf{P}}_{z_1})$, $\hat{\hat{\mathbf{p}}}_{z_2} = \text{vec}(\hat{\mathbf{P}}_{z_2})$, $\hat{A}'_{z_2} = \mathbf{I}_{Q_{g^c}} \otimes \hat{\mathbf{H}}_{g_m,f} \mathbf{V}^H_{z_2} \mathbf{U}_{z_2} \mathbf{V}_{z_2} \hat{\mathbf{H}}^H_{g_m,f}$, $\hat{A}_{z_2} = \mathbf{I}_{Q_{g_m}} \otimes \hat{\mathbf{H}}_{g_m,f} \mathbf{V}^H_{z_2} \mathbf{U}_{z_2} \mathbf{V}_{z_2} \hat{\mathbf{H}}^H_{g_m,f}$, $\hat{A}_{z_1} = \mathbf{I}_{Q_{g_m}} \otimes \hat{\mathbf{H}}_{g_m,f} \mathbf{V}^H_{z_1} \mathbf{U}_{z_1} \mathbf{V}_{z_1} \hat{\mathbf{H}}^H_{g_m,f}$, $\hat{\mathbf{a}}_{z_1} = \text{vec}(\mathbf{U}_{z_1} \hat{\mathbf{H}}_{g_m,f} \mathbf{V}^H_{z_1})$, $\hat{\mathbf{a}}_{z_2} = \text{vec}(\mathbf{U}_{z_2} \hat{\mathbf{H}}_{g_m,f} \mathbf{V}^H_{z_2})$, $\boldsymbol{\rho}_{z_1} = \sigma^2_{z_1} \text{tr}(\mathbf{U}_{z_1} \mathbf{V}_{z_1} \mathbf{V}^H_{z_1}) + \text{tr}(\mathbf{U}_{z_1}) + \log\det(\mathbf{U}_{z_1})$, and $\boldsymbol{\rho}_{z_2} = \sigma^2_{z_2} \text{tr}(\mathbf{U}_{z_2} \mathbf{V}_{z_2} \mathbf{V}^H_{z_2}) + \text{tr}(\mathbf{U}_{z_2}) + \log\det(\mathbf{U}_{z_2})$. The proposed AO algorithm for resource allocation and sum-rate maximization is outlined in Algorithm 1

V. Numerical Evaluation and Discussion

In this section, we present the simulation evaluation against several benchmarks to prove its efficacy. For the simulation en-

$$\underset{\hat{\chi}}{\text{maximize}} \sum_{g=1}^{G}\sum_{m=1}^{M_g}\frac{\tau}{S_g}\sum_{f\in\mathcal{S}_g}\delta_{g_m^c,f}+\xi_{z_1,f} \text{ subject to (12a)}, \sum_{j=1,j\neq m}^{M_g}\delta_{g_j^c,f}\geq\xi_{g_m^c,f} \text{ (17b), and } \delta_{g_m^c,f}\leq 0 \text{ (17c)}, \tag{17}$$

$$\underset{\mathbf{P}_{g^c,f},\mathbf{P}_{g_m^p,f},\delta_{g_m^c,f}}{\text{maximize}} \sum_{g=1}^{G}\frac{\tau}{S_g}\sum_{f\in\mathcal{S}_g}\sum_{m=1}^{M_g}(\delta_{g_m^c,f}+\boldsymbol{\rho}_{z_1}+\hat{\mathbf{p}}_{z_1}^H\hat{\mathbf{A}}_{z_1}\hat{\mathbf{p}}_{z_1}+\sum_{i\neq m}^{M_g}\hat{\mathbf{p}}_{\hat{z}_1}^H\hat{\mathbf{A}}_{z_1}\hat{\mathbf{p}}_{\hat{z}_1}-\hat{\mathbf{a}}_{z_1}^H\hat{\mathbf{p}}_{z_1}-\hat{\mathbf{p}}_{z_1}^H\hat{\mathbf{a}}_{z_1})$$

$$\text{subject to}\sum_{g=1}^{G}\sum_{f\in\mathcal{S}_g}[\sum_{m=1}^{M_g}\text{tr}(\hat{\hat{\mathbf{p}}}_{z_1}^H\hat{\hat{\mathbf{p}}}_{z_1})+\text{tr}(\hat{\hat{\mathbf{p}}}_{z_2}^H\hat{\hat{\mathbf{p}}}_{z_2})]\leq P_T \text{ (19a)}, \delta_{m}^{c},_f\leq 0 \text{ (19b)} \tag{19}$$

$$\sum_{m=1}^{M_g}\sum_{f\in\mathcal{S}_g}\delta_{g_m^c,f}+\sum_{f\in\mathcal{S}_g}Q_{z_2}\geq\sum_{f\in\mathcal{S}_g}\hat{\hat{\mathbf{p}}}_{z_2}^H\hat{\mathbf{A}}_{z_2}^{'}\hat{\hat{\mathbf{p}}}_{z_2}+\sum_{f\in\mathcal{S}_g}\boldsymbol{\rho}_{z_2}+\sum_{f\in\mathcal{S}_g}\sum_{i=1}^{M_g}\hat{\hat{\mathbf{p}}}_{\hat{z}_1}^H\hat{\mathbf{A}}_{z_2}\hat{\hat{\mathbf{p}}}_{\hat{z}_1}-\sum_{f\in\mathcal{S}_g}\hat{\mathbf{a}}_{z_2}^H\hat{\hat{\mathbf{p}}}_{z_2}-\sum_{f\in\mathcal{S}_g}\hat{\hat{\mathbf{p}}}_{z_2}^H\hat{\mathbf{a}}_{z_2} \text{ (19c)}$$

TABLE I
SIMULATION VARIABLE DEFINITIONS AND VALUES.

Variable	Value	Variable	Value	Variable	Value	Variable	Value	Variable	Value
h_{BS}	25m	h_{vehicle}	1.5m	bandwidth	20×10^6Hz	C	3×10^8m/s	f_c	6×10^9Hz
F	256	N_{BS}	60	$N_{\text{BS},k}$	4	$N_{\text{V},l}$	2	K	20
$\{P_T, P_{T,g_m}\}$	$\{30,20\}$dBm	$\sigma^2_{g_m}$	-130dBm	$\sigma^2_{g_{m,l}}$	-130dBm	τ	0.5	L	2

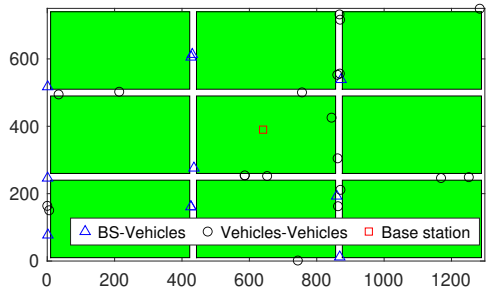

Fig. 3. 2D topology example of the proposed system model

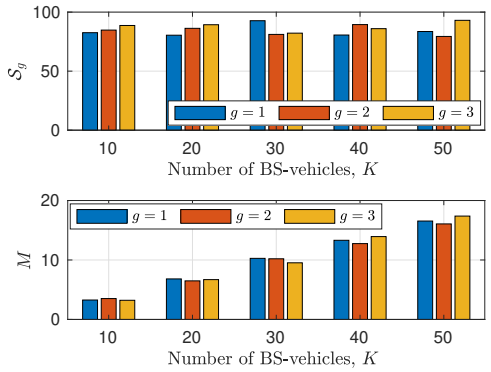

Fig. 4. Sub-carrier allocation and user-grouping algorithm performance

vironment, we consider both the urban grid and pathloss models described in the 3GPP standards with simulated topology shown in Fig. 3 [16], [17]. With the large-scale fading channel model component, for the BS to vehicle pathloss model, the urban macro (UMa) pathloss model is adopted, while for the vehicle to vehicle channel model, the V2V sidelink pathloss model is adopted [16], [17]. The Rician channel model was adopted for the general small-scale channel model. The details simulation parameters are presented in Table . Each simulation is generated using 10^3 channel randomization. For comparison, the multi-carrier space division multiple access (MC-SDMA) (SDMA Opt.), and fixed transmit powers MC-RSMA (RSMA Fix) and MC-SDMA (SDMA Fix) are used as benchmarks in the simulation.

Fig. 4 shows the performance of the user grouping and sub-carrier allocation algorithms with increasing number of vehicles communicating with the BS. The top bar graph is the number of sub-carriers ($\mathcal{S}_g$) allocated to each group, while the bottom bar graph shows the number of users (M_g) within each group. It is observed that with increasing K, the vehicles (M_g) within a group creases. Unlike the M_g bar graph, the sub-carriers allocated to a group does not follow a similar pattern. Additionally, both the users and sub-carriers allocated

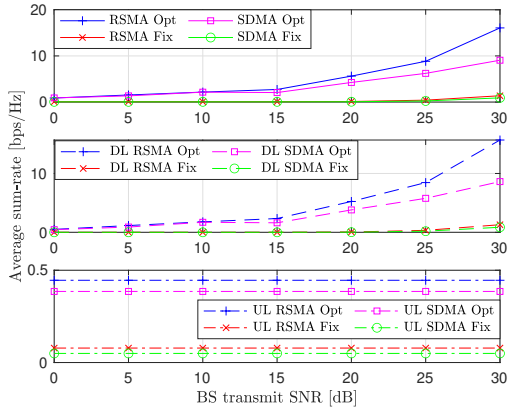

Fig. 5. Average sum-rate against BS power

to a group does not have a specific pattern observed, because, both bar graphs and allocation schemes depend on the channel characteristics.

Fig. 5 contains the sum-rate performance plot of the RSAM-MV2X system with increasing BS transmit power (P_T). Both the total system sum-rate and DL sum-rate increase with

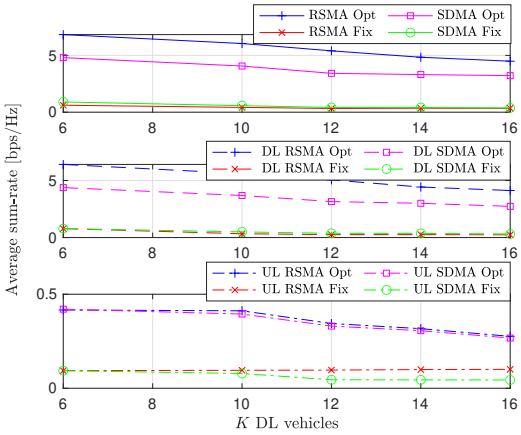

Fig. 6. Average sum-rate versus number of DL vehicles

increasing P_T, but the DFUS (UL) sum-rate remains constant since its not influenced by P_T. DFUS sum-rate values have a difference of 0.1 bps/Hz and 10^-3bps/Hz between the optimal (RSMA-SDMA) and fixed (RSMA-SDMA) approaches, respectively. The very low sum-rate values is due to the large interferences present because of other vehicles private and common messages present during desired signal decoding. The total sum-rate and DL sum-rate have the same pattern due to the large influence of the DL sum-rate, because it has lesser interference compared to the DFUS sum-rate. Hence, developing an approach to mitigate the DFUS interference will improve the system performance.

The effects of increasing the number of vehicles, K, communicating with the BS in DL on the system sum-rate is depicted in Fig. 6. Note, each DL vehicle is assigned two vehicles for its sidelink communication. The optimal RSMA approach has a "constant" performance of 1 bps/Hz over the optimal SDMA approach for both the total sum-rate and DL sum-rate. However, their fixed versions have marginal differences of about 0.01 bps/Hz. It can be observed that the sum-rate decreases (differences of about 2 bps/Hz and 10^-3 bps/Hz for the optimal and fixed schemes) with increasing number of vehicles. The DFUS (UL) sees very low sum-rate (less than 0.5 bps/Hz) values due to the presence of the common messages present during private data decoding. This is due to the increase in interference due to other users present within the network and the fixed BS transmit power. The fixed BS power is first shared among the sub-carrier, and each sub-carrier power is shared among the vehicles allocated to that sub-carrier. The more the vehicles assigned to a sub-carrier, the lesser the sub-carrier power allocated to each vehicle. This affects their achievable rates and the interferences from the co-grouped vehicles sharing the sub-carriers. The co-grouped vehicles have their common messages serving as additional interferences within the RSMA schemes, compared to the SDMA scheme. However, the RSMA approach has the common rate adding to its private rates.

VI. Conclusion

In this work, we proposed the promising two-way MC-RSMA MV2X communication ecosystem supporting vehicle DL and vehicle-BS DFUS communication. We proposed a k-mean DL vehicles grouping, a suboptimal sub-carrier allocation, and optimal beamforming algorithm for the proposed system with sum-rate as the performance metric. The proposed algorithm outperformed the MC-SDMA benchmark showing how promise our proposed system holds. We will consider incorporating symbiotic radio and joint sensing and communication systems into the system model for an efficient spectrum and power usage in future work.

References

[1] W. Anwar, N. Franchi, and G. Fettweis, "Physical layer evaluation of V2X communications technologies: 5G NR-V2X, LTE-V2X, IEEE 802.11bd, and IEEE 802.11p," in *Proc. IEEE Veh. Technol. Conf.* IEEE, Sep. 2019, pp. 1–7.

[2] M. H. C. Garcia, A. Molina-Galan, M. Boban, J. Gozalvez, B. Coll-Perales, T. Şahin, and A. Kousaridas, "A tutorial on 5G NR V2X communications," *IEEE Commun. Surveys & Tut.*, vol. 23, no. 3, pp. 1972–2026, Feb. 2021.

[3] M. Noor-A-Rahim, Z. Liu, H. Lee, M. O. Khyam, J. He, D. Pesch, K. Moessner, W. Saad, and H. V. Poor, "6G for vehicle-to-everything (V2X) communications: Enabling technologies, challenges, and opportunities," *Proceedings of the IEEE*, pp. 1–23, May 2022.

[4] S. Yoshioka and S. Nagata, "Cellular V2X standardization in 4G and 5G," *IEICE Trans. Fundamentals of Electronics, Commun. Computer Sciences*, no. 5, pp. 754–762, Nov. 2022.

[5] Z. Ali, S. Lagén, L. Giupponi, and R. Rouil, "3GPP NR V2X mode 2: overview, models and system-level evaluation," *IEEE Access*, vol. 9, pp. 89 554–89 579, Jun. 2021.

[6] O. Dizdar, Y. Mao, and B. Clerckx, "Rate-splitting multiple access to mitigate the curse of mobility in (massive) MIMO networks," *IEEE Trans. Commun.*, vol. 69, no. 10, pp. 6765–6780, Jul. 2021.

[7] C. Xu, B. Clerckx, S. Chen, Y. Mao, and J. Zhang, "Rate-splitting multiple access for multi-antenna joint radar and communications," *IEEE J. Sel. Topics Sig. Process.*, vol. 15, no. 6, pp. 1332–1347, Sep. 2021.

[8] L. Yin and B. Clerckx, "Rate-splitting multiple access for dual-functional radar-communication satellite systems," in *Proc. IEEE Wireless Commun. Network. Conf.* IEEE, May 2022, pp. 1–6.

[9] O. Dizdar, A. Kaushik, B. Clerckx, and C. Masouros, "Energy efficient dual-functional radar-communication: Rate-splitting multiple access, low-resolution DACs, and RF chain selection," *arXiv preprint arXiv:2202.09128*, Feb. 2022.

[10] R. C. Loli, O. Dizdar, and B. Clerckx, "Rate-splitting multiple access for multi-antenna joint radar and communications with partial CSIT: Precoder optimization and link-level simulations," *arXiv preprint arXiv:2201.10621*, Jan. 2022.

[11] L. Li, K. Chai, J. Li, and X. Li, "Resource allocation for multicarrier rate-splitting multiple access system," *IEEE Access*, vol. 8, pp. 174 222–174 232, Sep. 2020.

[12] O. Dizdar and B. Clerckx, "Rate-splitting multiple access for communications and jamming in multi-antenna multi-carrier cognitive radio systems," *IEEE Trans. Info. Forensics Security*, vol. 17, pp. 628–643, Feb. 2022.

[13] S. Jacobsson, G. Durisi, M. Coldrey, and C. Studer, "Linear precoding with low-resolution DACs for massive MU-MIMO-OFDM downlink," *IEEE Trans. Wireless Commun.*, vol. 18, no. 3, pp. 1595–1609, Jan. 2019.

[14] A. Mishra, Y. Mao, O. Dizdar, and B. Clerckx, "Rate-splitting multiple access for downlink multiuser MIMO: Precoder optimization and PHY-layer design," *IEEE Trans. Commun.*, no. 2, Feb. 2021.

[15] Z. Shen, J. G. Andrews, and B. L. Evans, "Adaptive resource allocation in multiuser OFDM systems with proportional rate constraints," *IEEE Trans. Wireless Commun.*, vol. 4, no. 6, pp. 2726–2737, Nov. 2005.

[16] TR37.885, "Technical specification group radio access network; Study on evaluation methodology of new Vehicle-to-Everything (V2X) use cases for LTE and NR;(release 16)," 3rd Generation Partnership Project, techreport, Jun. 2019.

[17] 3GPP, "TR 38.901 V17.0.0: Study on channel model for frequencies from 0.5 to 100 GHz, (Release 17)," pp. 26–29, Mar. 2022.